

Phase trajectories of fluid control volumes in a system with Benard-Rayleigh convection

A.S. Fedotov¹, Y.D. Tsitavets¹, Y.Levy²

1. Computer Modelling Department, Physics Faculty, Belarusian State University, Minsk, Republic of Belarus;

2. Scientific Laser Applications Department, HiLASE Centre, Institute of Physics of the Czech Academy of Sciences, Za Radnicí 828, 2524 Dolní Brežany, Czech Republic.

Introduction

Benard-Rayleigh convection is a formation of stable circulation contours in a fluid that moves between two horizontal plates heated from below. This phenomenon attracts the attention of researchers from both applied [1,2] and fundamental [3,4] areas. The significant progress in the description of Benard-Rayleigh convection was achieved using the Lorentz system of ordinary differential equations, which led to the development of the strange attractor concept [5]. However, the analysis of the Lorentz system implies simplifications: the independence of the fluid properties on temperature (except for the density) and the keeping of only lower-order terms in the Fourier representation of the stream function [6]. The computational capabilities of computers and the availability of software codes in recent years make it possible to study the dynamics of Benard-Rayleigh convection using the computationally-intensive Navier-Stokes equations that do not have the restrictions above.

Phase portraits analysis is a useful method to represent the directional behavior of ordinary equations systems [7]. To plot the phase portrait for a Navier-Stokes system, one has to introduce ordinary equations of motion for the fluid control volumes. If Navier-Stokes equations are solved using Lagrangian formulation [8] it can be done by simply tracking the Lagrangian coordinates. However, the majority of software including COMSOL uses the Eulerian formulation. This approach leads to the need for additional equations of motion for fluid control volumes. In the framework of COMSOL, it can be implemented using the Particle Tracing Module with massless particles. The particles' velocities at every coordinate and time moment are coincident with the correspondent velocity of fluid computed from Navier-Stokes equations.

In this paper, we explore the possibilities of phase space analysis to studying the Benard-Rayleigh convective flow using the numerical solution of the Navier-Stokes equations and equations of motion for massless particles.

Mathematical model

Benard-Rayleigh convection can be described using incompressible Navier-Stokes equations with an additional equation for heat transfer in Boussinesq approximation:

$$\begin{aligned} \frac{\partial \vec{v}}{\partial t} + (\vec{v} \nabla \vec{v}) &= -\frac{1}{\rho_0} \nabla P + \nu \Delta \vec{v} - \vec{g} \beta T, \\ \operatorname{div} \vec{v} &= 0, \\ \frac{\partial T}{\partial t} + (\vec{v} \nabla) T &= \chi \Delta T, \end{aligned} \quad (1)$$

where \vec{v} is velocity, P is pressure, ρ_0 is the density of fluid at characteristic temperature T_0 , ν is kinematic viscosity, \vec{g} is free-fall acceleration, β is volume expansion coefficient, χ is heat diffusivity. Archimedes buoyant force is accounted for by the term $\vec{g} \beta T$ in the momentum equation.

Boussinesq approximation establishes the linear dependence of fluid density on the temperature:

$$\rho(T) = \rho_0(1 - \beta\theta), \quad (2)$$

where $\theta = T - T_0$.

The following boundary and initial conditions were set:

$$\begin{cases} T = T_{hot}, y = 0, x \in \Gamma \\ T = T_{cold}, y = y_{max}, x \in \Gamma \\ -\vec{n} \cdot \lambda \nabla T = 0, x = 0, y \in \Gamma \\ -\vec{n} \cdot \lambda \nabla T = 0, x = x_{max}, y \in \Gamma \\ \vec{v} = 0, (x, y) \in \Gamma \\ \vec{v}|_{t=0} = 0, (x, y) \in \Omega \\ T|_{t=0} = T_0, (x, y) \in \Omega \end{cases}, \quad (3)$$

where Ω is the computational domain, Γ is the boundary of the domain, x_{max} is the maximal value of x -coordinate in the domain, y_{max} is the maximal value of y -coordinate in the domain, λ is the heat conduction coefficient, \vec{n} is the local normal to Γ .

Massless particles with coordinates q_i were uniformly distributed inside the computational domain (Figure 1). After Navier-Stokes solution reaches stationary state we begin to integrate the equations of motion:

$$\frac{d\vec{q}_i}{dt} = \vec{v}(\vec{q}_i, t). \quad (4)$$

The equation (4) states that equations of motion for particles are being solved simultaneously with equations (1) and the velocity of each particle is defined only by a fluid velocity in the same point of space. Note, that the resulting trajectories are different from the standard streamlines. Streamlines are usually being integrated over the velocity field at a fixed time moment, and Eqs. (4) are considering the time-dependent velocity field, taking into account periodical fluctuations and quasiperiodicity. Such an approach allows obtaining the trajectories fully matching with trajectories of fluid control volumes in the Lagrangian formulation.

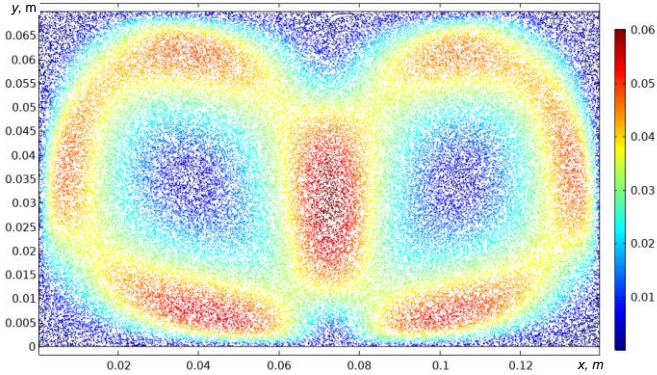


Figure 1. Initial spatial distribution of massless particles released inside of the computational domain. Color indicates the particle velocity magnitude.

Numerical methods

The Navier-Stokes equations were solved as implemented via the CFD Module (laminar). Velocity was discretized using parabolic basis functions, both pressure and the temperature were discretized using linear functions. Backward differentiation formula of 3rd order was used for time integration and PARDISO solver [9] was used for the solution of systems of linear equations.

Particle tracing was performed with the Particle Tracing Module. Equations of motion were integrated using the Dormand-Prince method [10].

The computational mesh had 10^4 elements including 10^2 boundary elements. Mesh becomes denser near the wall to better resolve the flow in the boundary layers.

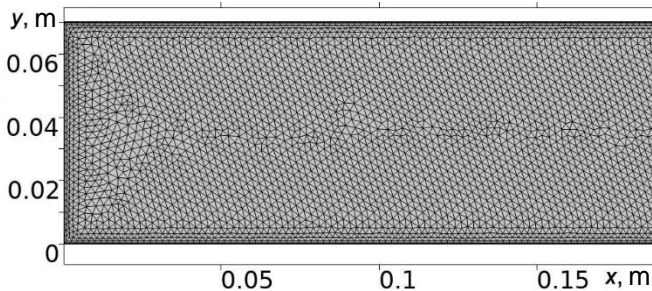


Figure 2. Fragment of the computational mesh.

Results and discussion

The Rayleigh number [6] defines the behavior of the system with convective heat transfer:

$$Ra = \frac{g\beta(T_{hot} - T_{cold})L^3}{\nu\chi}, \quad (5)$$

where L is the distance between the hot and cold boundary.

In the range of Rayleigh number $Ra = 10^2 - 10^6$, the two-dimensional flow for such a system qualitatively remained similar. We focused on $Ra = 2 \cdot 10^5$ as it provides faster convergence to the stationary state.

The material parameters such as viscosity, expansion coefficient, heat diffusivity, and heat conduction coefficient were set corresponded to air. The temperature difference between the hot and cold boundaries was 5.5 K, the initial temperature of the domain was coinciding with the $T_{cold} = 293.15$ K.

The stationary state was reached in 40 s of simulated time. The found flow characteristics in a single convective cell are given in Figure 3. The cell is established to consist of a pair of vortices rotating in opposite directions (Fig.3a,c). Hot air rises due to the buoyancy force and drag by vortices in the center of the convective cells (Fig 2b). This is in coincidence with existing physical concepts [11].

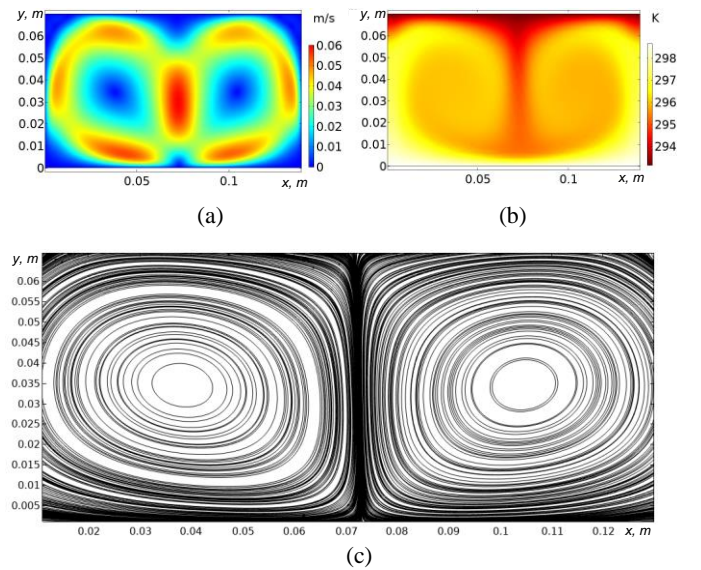


Figure 3. Spatial distribution of Benard-Rayleigh flow characteristics at a stationary state for $Ra = 2 \cdot 10^5$: (a) – velocity magnitude, (b) – temperature, (c) – streamlines.

The height dependences of the flow characteristics inside one of the vortices are given in Figure 4. After the flow stabilization at 40 s, both x - and y -components of the velocity become symmetrical about the center of the vortex (Fig.4a).

The temperature distribution inside the vortex was found to be almost uniform (Fig.4b). The noticeable changes of the temperature occur only between the vortex edges and the hot (or cold) boundary.

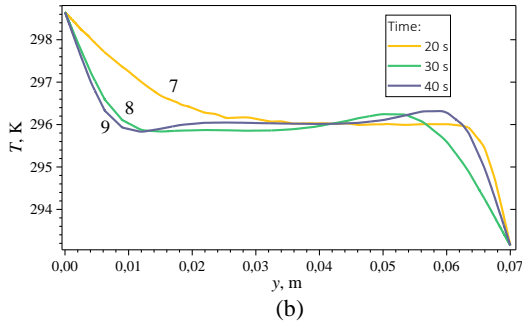
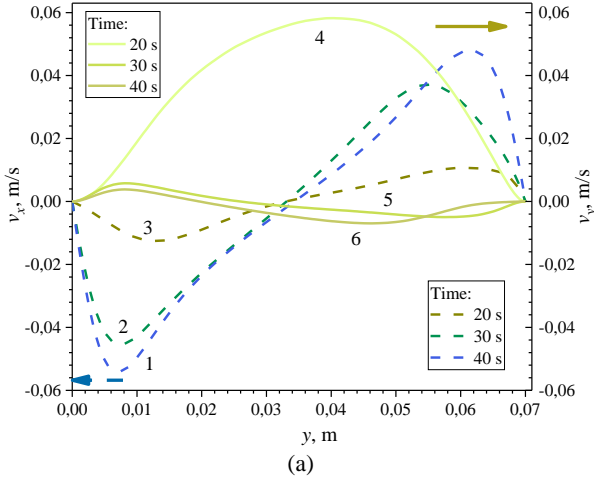


Figure 4. Dependence of (a) x - and y -components of velocity and (b) temperature on y inside a vortex in different time moments. 1, 2, 3 – v_x at 20, 30 and 40 s; 4, 5, 6 – v_y at 20, 30 and 40 s; 7, 8, 9 – T at 20, 30 and 40 s, respectively.

To analyze the phase space of the system we placed 80 000 massless particles into the computational domain. The integration of equations of motion was coupled with the time-integration of the Navier-Stokes equation.

We built the new “Particles” dataset in the “Datasets” node of the “Results” section of COMSOL. The geometry of the particles was based on the transient study solution for Particle Tracing interface. The position-dependent variables were changed from the standard (qx, qy) to (qx, qxt) or (qy, qyt) . This allows us to plot the particles in phase space using all the standard COMSOL functionality for visualization of particles.

Phase portraits for 80 000 particles are given in Figure 5. The portraits show stability and possess a constant smooth envelope both in (qx, qxt) coordinates (Fig.5a) and (qy, qyt) coordinates (Fig.5b).

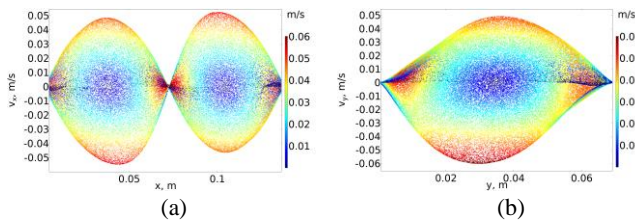


Figure 5. Phase portraits for massless particles ensemble (a) in coordinates (qx, qxt) and (b) in coordinates (qy, qyt) . Color indicates the velocity magnitude of the particles.

Trajectories of particles in (qx, qxt) for a single convective cell are given in Figure 6. It can be seen that particles can be divided into two groups.

The first group consists of the particles with trajectories rotating about the two centers divided by the stationary manifold. Points of this group cannot transit from the orbit around one of the centers to the orbit around another one. A similar picture is observed for phase trajectories in (qy, qyt) coordinates.

The second group consists of the particles which can pass through the common point between the neighborhoods of the two centers. These particles are characterized by a temperature close to the highest or the lowest temperature in the whole system (Fig.6). These particles in real space move in the boundary layers near the hot or the cold wall and do not belong to stable vortices rotating with the same angular velocity.

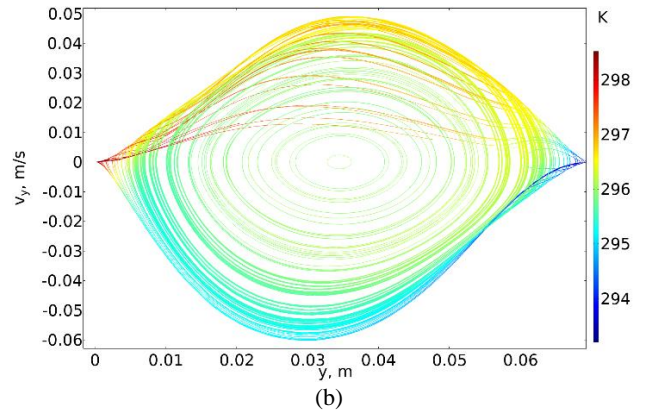
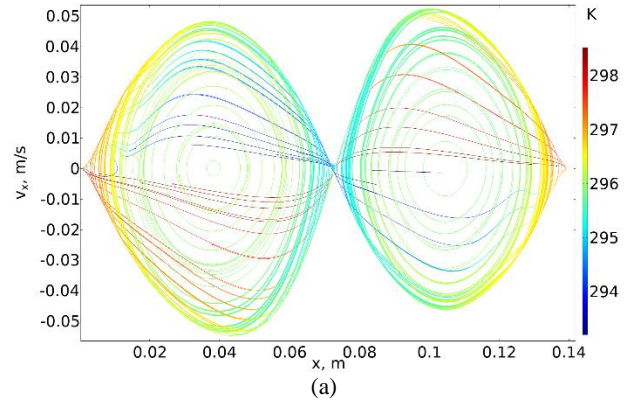


Figure 6. Phase trajectories for massless particles (a) in coordinates (qx, qxt) and (b) in coordinates (qy, qyt) . Color: local temperature of the particle.

The kinetic energy of each particle in arbitrary units can be estimated as the square of velocity magnitude. The energy distribution over all particles is given in Figure 7a. We can see three characteristic peaks on the histogram. In order to understand the role of these peaks we colored the particles in the domain with color related to each peak (Fig 7b).

The first peak with the smallest energy is attributed to the almost non-moving particles near the walls and in the centers of vortices. The middle-energy peak is related to the particles on the boundary of the vortices which are also

influenced by the non-moving particles near the walls. The high-energy peak is attributed to the characteristic energy of particles in the vortex away from the walls and the non-moving vortex centers.

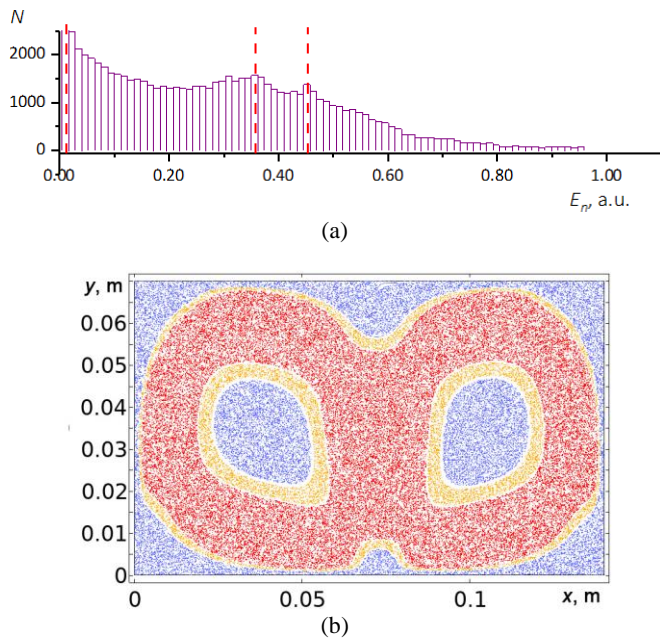


Figure 7. Energy distribution over the particles: (a) histogram over the normalized energy and (b) particles in the domain colored in the dependence of their energy: blue color – lowest energy peak, orange color – medium energy peak, red color – highest energy peak.

Conclusions

A new method for the construction of system phase portraits was developed. The method uses the embedded functionality of COMSOL and provides a simple and robust approach for the analysis of systems described by the Navier-Stokes equations. The main idea of the method is the introduction of massless particles into the flow area with velocities coinciding with the local velocity of the fluid. Such particles represent the control volume of fluid. The further analysis of particles' trajectories allows building the phase portraits.

This method was tested on a system with Benard-Rayleigh convection with $Ra = 2 \cdot 10^5$. It was shown that phase trajectories of the fluid control volumes in such a system may be divided into two groups. The first group represents particles that are rotating around the special point centers. The second group represents particles with a very high and low temperature in a system that can freely transit between two stable neighborhoods of the above-mentioned centers.

The analysis of massless particles allows the analysis of the characteristic kinetic energy of the flow. Energy distribution in Benard-Rayleigh convection showed three peaks. The first peak with the smallest energy is related to the particles near the walls, the second peak is attributed to the outer boundary of the vortices and the third peak marks the characteristic energy of the vortex away from the walls and the vortex center.

References

1. M. Lappa, *Rotating Thermal Flows in Natural and Industrial Processes*. John Wiley & Sons, Ltd, Chichester, West Sussex (2012).
2. G. Ahlers, S. Grossmann, and D. Lohse, Heat Transfer and Large Scale Dynamics in Turbulent Rayleigh-Bénard Convection, *Rev. Mod. Phys.* **81**, 503 (2009).
3. X. Shan, Simulation of Rayleigh-Bénard Convection Using a Lattice Boltzmann Method, *Phys. Rev. E - Stat. Physics, Plasmas, Fluids, Relat. Interdiscip. Top.* **55**, 2780 (1997).
4. Y. R. Li, Y. Q. Ouyang, L. Peng, and S. Y. Wu, Direct Numerical Simulation of Rayleigh-Bénard Convection in a Cylindrical Container of Aspect Ratio 1 for Moderate Prandtl Number Fluid, *Phys. Fluids* **24**, 074103 (2012).
5. J. Guckenheimer and C. Sparrow, The Lorenz Equations: Bifurcations, Chaos, and Strange Attractors., *Am. Math. Mon.* **91**, 325 (1984).
6. P. G. Frick, *Turbulence: Approaches and Models (in Russian)*, 2nd ed. Izhevsk: Institute of Computer Science, Moscow (2010).
7. J. C. Butcher, *Numerical Methods for Ordinary Differential Equations*. Wiley Blackwell (2016).
8. A. Bennett, *Lagrangian Fluid Dynamics*. Cambridge University Press (2006).
9. D. Kourounis, A. Fuchs, and O. Schenk, Toward the Next Generation of Multiperiod Optimal Power Flow Solvers, *IEEE Trans. Power Syst.* **33**, 4005 (2018).
10. P. J. Prince and J. R. Dormand, High Order Embedded Runge-Kutta Formulae, *J. Comput. Appl. Math.* **7**, 67 (1981).
11. R. Karwa, *Heat and Mass Transfer*. Springer Singapore (2017).

Acknowledgments

The authors gratefully acknowledge support by the project H2020-MSCA-RISE "ATLANTIC" (GA 823897).